Research Article J. Electrochem. Sci. Technol., 2022, 13(4), 453-461

Low-Temperature Chemical Sintered TiO_2 Photoanodes Based on a Binary Liquid Mixture for Flexible Dye-Sensitized Solar Cells

Md. Mahbubur Rahman[1], Hyeong Cheol Kang[2], Kicheon Yoo[2], and Jae-Joon Lee[2]*

[1]*Department of Applied Chemistry, Konkuk University, Chungju 27478, Korea*

[2]*Department of Energy Materials Science and Engineering, Research Center for Photoenergy Harvesting & Conversion Technology (phct), Dongguk University, Seoul 04620, Korea*

ABSTRACT

A chemically sintered and binder-free paste of TiO_2 nanoparticles (NPs) was prepared using a binary-liquid mixture of 1-octanol and CCl_4. The 1:1 (v/v) complex of CCl_4 and 1-octanol easily interacted chemically with the TiO_2 NPs and induced the formation of a highly viscous paste. The as-prepared binary-liquid paste ($\mathbf{P_{BL}}$)-based TiO_2 film exhibited the complete removal of the binary-liquid and residuals with the subsequent low-temperature sintering (~150ºC) and UV-O_3 treatment. This facilitated the fabrication of TiO_2 photoanodes for flexible dye-sensitized solar cells (*f*-DSSCs). For comparison purposes, pure 1-octanol-based TiO_2 paste ($\mathbf{P_O}$) with moderate viscosity was prepared. The $\mathbf{P_{BL}}$-based TiO_2 film exhibited strong adhesion and high mechanical stability with the conducting oxide coated glass and plastic substrates compared to the $\mathbf{P_O}$-based film. The corresponding low-temperature sintered $\mathbf{P_{BL}}$-based *f*-DSSC showed a power conversion efficiency (PCE) of 3.5%, while it was 2.0% for $\mathbf{P_O}$-based *f*-DSSC. The $\mathbf{P_{BL}}$-based low- and high-temperature (500ºC) sintered glass-based rigid DSSCs exhibited the PCE of 6.0 and 6.3%, respectively, while this value was 7.1% for a 500ºC sintered rigid DSSC based on a commercial (or conventional) paste.

Keywords : Dye-sensitized solar cells, Raoult's law, Binder-free TiO_2 paste, 1-Octanol, Carbon tetrachloride, Low-temperature, High viscosity

Received : 29 March 2022, Accepted : 21 June 2022

1. Introduction

Since the invention of dye-sensitized solar cells (DSSCs) in 1991, extensive research has been performed to understand the operation principle and improve the power conversion efficiency (PCE) [1-3]. As a consequence, the PCE of over 14% was achieved for conventional glass/fluorine-doped tin oxide (FTO) substrate and high-temperature (500ºC) sintered TiO_2 photoanode-based rigid DSSCs (*g*-DSSCs) [4,5]. The fabrication of TiO_2 photoanodes under low-temperature (150ºC or lower temperature range) sintering conditions for DSSCs application has attracted substantial interest over the conventional high-temperature sintering process. This is advantageous not only for the fabrication cost reduction but also for developing mobile power sources for wearable electronic and IoT devices with lightweight and flexibility [6,7]. Additionally, the low-temperature fabrication method can be applicable for preparing multilayer structures with different dyes at each layer that can facilitate the PCE enhancement by solar spectrum splitting in the course of light passage through the photoanode [8].

The preparation of TiO_2 photoanodes for conventional high-efficiency *g*-DSSCs fabrication requires the use of organic binders such as polyethylene glycol, ethylcellulose, and hydroxypropyl cellulose. These binders increase the viscosity of the TiO_2 pastes and enable the preparation of highly stable, crack-free, and homogenous mesoporous TiO_2 (mp-TiO_2) films with a thickness of > 10 μm [9,10]. During the sintering process at 500ºC, these organic binders are burned out and facilitate the formation of mp-TiO_2 layers. In addition, this process induces the

*E-mail address: jjlee@dongguk.edu

DOI: https://doi.org/10.33961/jecst.2022.00262

development of excellent electrical pathways for transporting photo-injected electrons by improving the interparticle connection of TiO_2 and the adhesion of the TiO_2 layer with glass/FTO substrates [9-11]. However, the conventional binder containing TiO_2 pastes and the high-temperature sintering methods are unsuitable for fabricating transparent conducting oxide-coated plastic substrates-based flexible DSSC (*f*-DSSC) [8]. This is because flexible plastic substrates, indium tin oxide/polyethylene naphthalate (ITO/PEN) and ITO/polyethylene terephthalate (ITO/PET), cannot withstand a process at a temperature exceeding 150ºC [12].

So far, mechanical pressing [13,14], electrophoretic deposition [15-17], microwave sintering [18], spray-deposition [19], chemical sintering [20,21], and film transfer (lift-off) [22] methods have been demonstrated for fabricating low-temperature processed TiO_2 film onto the flexible substrates for DSSCs application. Among these methods, mechanical methods for TiO_2 film fabrication required complicated multi-step fabrication processes with additional post-treatment, and they were generally ineffective for preparing a TiO_2 film with a thickness of > 10 μm [7]. Additionally, these TiO_2 film fabrication methods result in imperfect TiO_2 NPs interconnections and poor adhesion of the TiO_2 film with the flexible plastic substrates, resulting in inefficient charge transfer and collection in *f*-DSSCs [7,23]. Contrary to the mechanical methods, the solution-processed chemical sintering approach is promising for fabricating low-temperature sintered TiO_2 pastes and the corresponding TiO_2 films onto flexible plastic substrates with reduced fabrication steps, low cost, and high enough film thickness [21,23]. Furthermore, the chemical sintering approach offers the advantages of large-scale production of TiO_2 film with improved mechanical stability [23]. Accordingly, chemical sintering approaches were reported to prepare binder-free TiO_2 pastes using nano-glue (5 nm TiO_2 particles), ethanol, ammonia, acid-base mixture, acids, and water [21,23-26].

Park *et al.* developed a binder-free TiO_2 paste using acid-base chemistry of CH_3COO^- and NH_4^+ in solution [21]. The flocculation formation of TiO_2 nanoparticles (NPs) induced by CH_3COO^- and NH_4^+ could enhance the viscosity by improving the interaction between the TiO_2 NPs. The resulting binder-free and chemically sintered TiO_2 photoanode exhibited a PCE of 2.55% in *g*-DSSCs [21]. In another report, Li *et al.* developed a nano-glue-based TiO_2 paste with a well-interconnected NPs network [23]. The nano-glue acts as a chemical sintering agent for TiO_2 NPs, in which the ample surface hydroxyl groups (-OH) of nano-glue are well mixed with the TiO_2 NPs and increase the viscosity of the paste. The corresponding low-temperature sintered DSSC, fabricated with a plastic substrate-based TiO_2 photoanode and a platinized glass/FTO substrate-based counter electrode (CE), exhibited a PCE of 5.43%.

Strong acids such as hexa-fluorotitanic acid (H_2TiF_6) and hydrochloric acid (HCl) were used for preparing low-temperature chemically sintered TiO_2 pastes for *f*-DSSCs [25,26]. The oxidizing nature of acids can increase the amounts of -OH groups on the TiO_2 surface and improve the TiO_2 interparticle connection with the subsequent dehydration reaction at the low-temperature sintering conditions. Holliman *et al.* prepared a low-temperature sintered TiO_2 paste using H_2SiF_6 as a chemical sintering agent with a PCE of 4.2% in DSSC based on ITO/PET photoanode substrate and glass/FTO based CE substrate [26]. In another report, Weerasinghe *et al.* used HCl as a chemical sintering agent for preparing TiO_2 film with a PCE of 5% in *f*-DSSC [26]. Although these acids pastes-based TiO_2 films showed good adhesion with the substrates, the possible chemical etching of the ITO and FTO conducting layer by the H_2TiF_6 and HCl can lower the fill factor (FF) and photocurrent of the DSSCs devices [26]. Therefore, it is essential to develop ITO and FTO corrosion-resistive TiO_2 pastes, which exhibit high enough viscosity with sufficient mechanical strength and thickness of the TiO_2 layers and strong adhesion to the conductive flexible plastic substrates after low-temperature sintering.

In this study, a novel binary-liquid mixture of carbon tetrachloride (CCl_4) and 1-octanol was used for preparing chemically sintered low-temperature TiO_2 paste for *f*-DSSCs. The unfavorable physical and chemical properties of CCl_4, including high volatility, low-boiling temperature (T_b=76.72ºC), and low viscosity (0.965 cP), were not suitable for the preparation of TiO_2 pastes. Thus, 1-octanol with high T_b (194.5ºC) and high-viscosity (7.36 cP) was introduced into the CCl_4 for preparing highly viscous, binder-free, and chemically and low-temperature sintered TiO_2 pastes. According to *Raoult's law* [27], the high T_b of 1-octanol could decrease by the low T_b of

CCl_4 and facilitate the preparation of TiO_2 films sintered at low temperature (≤ 150ºC). The formation of the 1-octanol-CCl_4 complex could easily interact with the TiO_2 NPs via hydrogen bonding. This induced the reduction of TiO_2 interparticle distance and enabled the preparation of high-viscous pastes. The as-prepared chemically sintered and low-temperature TiO_2 films exhibited good inter-particle connection and porosity, improved mechanical strength, and strong adhesion to the ITO/PEN and glass/FTO substrates. The 150ºC sintered *g*-DSSCs and *f*-DSSCs fabricated with this binary-liquid paste exhibited PCEs of 6.0 and 3.5%, respectively.

2. Experimental

2.1 Chemicals and reagents

All the reagents and solvents were purchased from Sigma-Aldrich (St. Louis, MO, USA). Cis-diisothiocyanato–bis(2,2'-bipyridyl-4,4′-dicarboxylato) ruthenium (II) bis(tetrabutylammonium) (N719) dye was purchased from Solaronix, Switzerland. ITO/PEN (13 Ω/sq.) and glass/FTO (8 Ω/sq.) were purchased from Peccell Technologies Inc (Japan) and Pilkington (USA), respectively.

2.2 Preparati on of the TiO_2 pastes

Before preparing the TiO_2 pastes, the TiO_2 powder (Degussa P25) was pre-treated with acetylacetone to minimize NPs aggregation [9]. Then, 1 g of pre-treated TiO_2 powder was mixed with two compositions of 1-octanol and CCl_4 (1:1 and 1:0 (v/v)) and stirred at room temperature (RT) for 6 h. Subsequently, the mixture was homogenized for another 30 min to obtain homogenous dispersion of TiO_2 NPs by using an ultrasonic horn. The mixture was heated again at 70ºC with stirring (300 rpm/s) for 24 h to obtain the high viscous pastes. The pastes were denoted hereafter as $\mathbf{P_{BL}}$ and $\mathbf{P_O}$, where the composition of 1-octanol and CCl_4 were 1:1 and 1:0 (v/v), respectively.

2.3 Fabrication of DSSCs devices

The as-prepared TiO_2 pastes were coated on flexible ITO/PEN and glass/FTO substrates by the doctor blade method and dried at RT. Then, the TiO_2 films were sintered at 150ºC for 60 min in an electric oven in the presence of air. Subsequently, the films were treated with UV-O_3 for 30 min. For comparison, the $\mathbf{P_{BL}}$ and a commercial binder containing TiO_2 paste ($\mathbf{P_C}$) (TTPH-20N, ENBKOREA Co., Ltd., Korea, particle size 20 nm) were used to prepare 500ºC sintered TiO_2 films on glass/FTO substrate according to a previously reported method [28]. The thickness of the $\mathbf{P_{BL}}$ and $\mathbf{P_O}$-based TiO_2 films was *ca.* 15.8 and 15.3 μm, respectively, while it was *ca.* 15.4 μm for $\mathbf{P_C}$-based TiO_2 photoanode. All the TiO_2 electrodes were dipped into the N719 dye solution (0.3 mM) in ethanol for 18 h. For the preparation of *f*-DSSCs CE, Pt was sputtered on ITO/PEN substrate for about 10 s. While for the preparation of *g*-DSSCs CEs, 5 mM chloroplatinic acid hexahydrate ($H_2PtCl_6 \cdot 6H_2O$) solution in ethanol was drop cast onto the glass/FTO substrate and sintered in an electric muffle furnace at 400ºC for 20 min in air. The dye-loaded photoelectrodes (active area *ca.* 0.25 cm^2) and Pt-CEs were sandwiched using 60-μm thick Surlyn film (Solaronix SA, Switzerland) as a spacer and sealing agent using a hot press. The electrolyte solution with the composition of 0.6 M 1,2-dimethyl-3-propylimidazolium iodide (DMPII), 0.1 M LiI, 0.1 M I_2, and 0.5 M 4-*tert*-butylpyridine (*t*BP) and 1 mM 4′,6-diamidino-2-phenylindole (DAPI) as an efficient energy relay dye (ERD) [29] were dissolved in 3-methoxypropionitrile (MPN) and injected into the cells through the drilled holes on the CEs. The holes were sealed by using surlyn film with cover glass.

2.4 Instrumentations

The viscosity of the TiO_2 pastes was measured with a viscometer (μVisc, Rheosense, Inc., USA). The thickness of the TiO_2 films was measured by a surface profilometer (Accretech, Japan), and the adhesion of TiO_2 film with FTO was evaluated by a scotch-tape scratch test. The strength of adhesion of the films was evaluated using a peel-off tester (Top-Tac 2000, Korea). The crystallographic pattern of TiO_2 was characterized with an X-ray diffractometer (XRD, Philips, X'pert, Netherland) using Cu K_a radiation. A field-emission scanning electron microscope (FE-SEM, JSM-6700F, JEOL) equipped with energy-dispersive X-ray spectroscopy (EDS) was used (EDS, INCAx-sight7421, Oxford Instruments) to characterize the surface morphology and elemental analysis of TiO_2 films. The amount of adsorbed dye onto the TiO_2 film was determined by desorbing the dye in a 0.1 M NaOH aqueous solution, and the absorption spectra of the desorbed dye solutions were

measured using a UV−Vis absorption spectrophotometer (Perkin-Elmer Lamda 35). A solar simulator (Polaronix® K201, McScience, Korea) with a 200 W Xenon lamp with the incident light intensity of 100 mW/cm^2 (AM 1.5 G) was used for the photovoltaic (PV) measurements of the DSSCs. A PV power meter (Polaronix® K101 LAB20, McScience, Korea) was used to measure the current density-voltage (*J-V*) characteristics of DSSCs. Incident photon-to-electron conversion efficiency (IPCE) spectra were obtained by an IPCE measurement system (Polaronix, K3100 Spectral IPCE, McScience) with a 300 W xenon lamp source. Electrochemical impedance spectra (EIS) were measured using an impedance analyzer (IM6ex, Zahner Zahner-Elektrik GmbH & Co. KG, Germany) in the frequency range from 10^5 to 0.1 Hz with the ac amplitude of 5 mV under open-circuit potential and dark conditions. The EIS spectra were analyzed with an appropriate equivalent circuit using Z-view software (Scribner Associates Inc., version 3.1). Thermogravimetric (TGA) analyses were performed with a Scinco TGA-N 1000 analyzer (Seoul, Korea) under ambient atmospheric conditions.

3. Results and Discussion

3.1. Mechanism of TiO_2 NPs interconnection

Fig. S1 presents the bar diagram of the T_b variation of the CCl_4 and 1-octanol mixture against their volume fraction. The T_b of the binary mixture was increased by increasing the volume fraction of 1-octanol that is in accordance with *Raoult's law* [27]. Considering the preparation of binder-free, low-temperature chemically sintered TiO_2 paste, and the composition of CCl_4 and 1-octanol complex formation [30], a 1:1 volume ratio is selected as the optimized composition, where the T_b of 1-octanol:CCl_4 (1:1 v/v) was 97ºC. The schematic illustration of the TiO_2 NPs inter-connections in the mp-TiO_2 film based on $\mathbf{P_{BL}}$ is presented in Scheme 1. In the mixture of 1-octanol, CCl_4, and TiO_2 NPs, 1-octanol and CCl_4 could easily form a complex with a 1:1 (v/v) ratio via hydrogen bonding (O-H·····C1-C) [30]. Subsequently, this complex could interact with the -OH groups on the TiO_2 NPs surface and form Ti-O-C-O-C_8H_{17} and Ti-O-C-O-Ti bonds by the elimination of HCl. This enabled to decrease in the TiO_2 interparticle distance and formed a viscous paste. In the subsequent heat treatment of the as-prepared TiO_2 NPs film at 150ºC, CO_2 and H_2O can be eliminated by the decomposition of hydrocarbon chains and the dehydration of -OH groups on the surfaces of TiO_2 NPs, respectively. This induces to interconnect the TiO_2 NPs through the Ti-O-C-O-Ti bonds. Finally, upon the UV-O_3 treatment, Ti-O-C-O-Ti bonds can be broken and the residual carbon can be eliminated in the form of CO_2 and O_2 [31], resulting in the further reduction of TiO_2 interparticle distance and forming a highly stable mp-TiO_2 network through Ti-O-Ti bonds. This induces the decoloring of the film, which can be attributed to the complete removal of the remaining organic residues, as shown in Fig. S2. Meanwhile, for the case of $\mathbf{P_O}$, TiO_2 NPs are homogeneously distributed into the 1-octanol due to the physical adsorption as well as the hydrogen bonding interaction between the -OH groups of TiO_2 and 1-octanol. Upon heat treatment of the as-prepared $\mathbf{P_O}$-based TiO_2 film at 150ºC, 1-octanol can effectively bridge the gap between TiO_2 NPs by dehydration process. Finally, in the UV-O_3 treatment, the residual 1-octanol and carbon can be eliminated as CO_2 and O_2 (Fig. S2), thus, facilitating the formation of TiO_2 film with moderate stability.

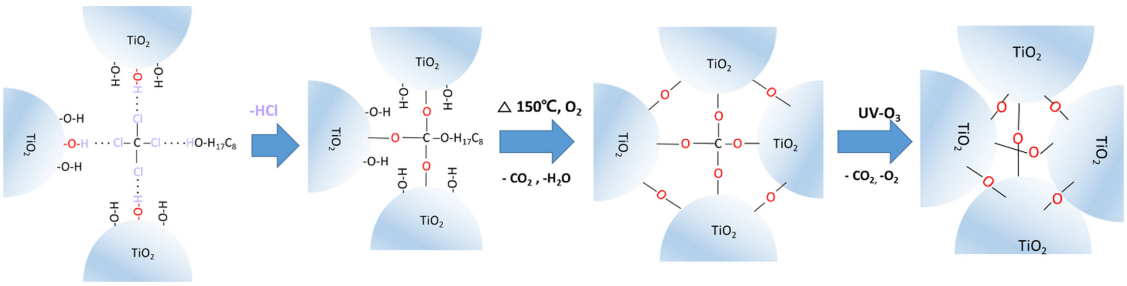

Scheme 1. Schematic illustrations of the TiO_2 interparticle connection in binary liquid-based TiO_2 paste via a dehydration process at 150ºC and subsequent UV-O_3 treatment.

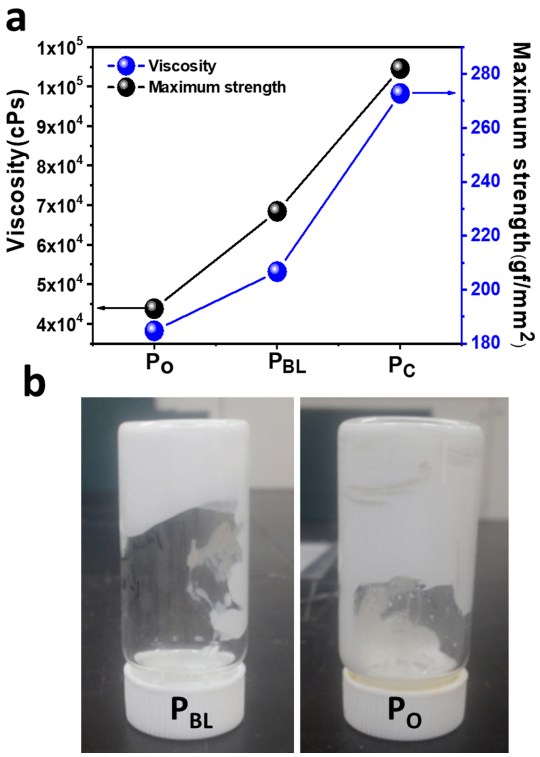

Fig. 1. (a) Viscosity of $\mathbf{P_{BL}}$, $\mathbf{P_O}$, and $\mathbf{P_C}$ pastes and the maximum strength of adhesion of their corresponding TiO_2 films onto glass/FTO substrates. (b) The photographic images of the as-prepared $\mathbf{P_{BL}}$ and $\mathbf{P_O}$.

3.2. Rheological behaviors

Fig. 1a shows the viscosity of the TiO_2 pastes ($\mathbf{P_{BL}}$, $\mathbf{P_O}$, and $\mathbf{P_C}$) and the mechanical strength of their corresponding TiO_2 films prepared onto the glass/FTO substrates by the doctor blade method. The corresponding photo-image of $\mathbf{P_{BL}}$ and $\mathbf{P_O}$ pastes is presented in Fig. 1b. The rheological behavior of the TiO_2 pastes revealed that the addition of CCl_4 with 1-octanol significantly increased the viscosity of the TiO_2 paste from 38,214 ($\mathbf{P_O}$) to 53,158 ($\mathbf{P_{BL}}$) cPs. This can be attributed to the hydrogen bonding between the TiO_2 NPs and the complex of CCl_4 and 1-octanol [30,32], which concurrently increase the maximum strength of adhesion of the 150ºC sintered TiO_2 film from 192 ($\mathbf{P_O}$) to 229 ($\mathbf{P_{BL}}$) gf/mm^2. These values were 98245 cPs and 282 gf/mm^2 for $\mathbf{P_C}$ under 500ºC sintering conditions. These results are consistent with the tape test results for the mechanical adhesion of $\mathbf{P_{BL}}$ compared to $\mathbf{P_O}$ (Fig. S3) on a glass/FTO substrate upon sintering at 150ºC followed by subsequent UV-O_3 treatment. $\mathbf{P_{BL}}$ showed the highest level of adhesion without affecting the cross-cut areas (~0%), while $\mathbf{P_O}$ exhibited a much lower degree of adhesion by detaching the cross-cut areas of ~10%.

3.3. Morphological, TGA, and XRD analyses

The morphology of TiO_2 films prepared from the $\mathbf{P_{BL}}$ and $\mathbf{P_O}$ was studied with FE-SEM. The TiO_2 film of $\mathbf{P_{BL}}$, before heat treatment at 150ºC, exhibited crack-free homogenous distribution of TiO_2 NPs with a relatively homogenous distribution of particle aggregation (Fig. S4a). In contrast, the TiO_2 film of $\mathbf{P_O}$ showed some cracks over the TiO_2 film with an enhanced particle aggregation by forming bigger local clusters over the film (Fig. S4b). After sintering at 150ºC and subsequent UV-O_3 treatment, the TiO_2 film of $\mathbf{P_{BL}}$ showed high porosity without the presence of NPs aggregation (Fig. 2a), while the TiO_2 film of $\mathbf{P_O}$ exhibited lower porosity with the presence of bigger local clusters over the film (Fig. 2b). The carbon content in the TiO_2 film of $\mathbf{P_{BL}}$ was analyzed by EDS under different treatment conditions (e.g., drying at 25ºC, 150ºC, 150ºC followed by UV-O_3 treatment, and 500ºC), as shown in Fig. 2c. The corresponding EDS spectra are presented in Fig. S5. It was observed that the carbon content in $\mathbf{P_{BL}}$ decreased significantly after both sintering at 150ºC and subsequent UV-O_3 treatment with a carbon content of 1.76%. This value for the RT dried and 150ºC sintered $\mathbf{P_{BL}}$-based TiO_2 films was 3.0 and 2.48%, respectively. Further, a small reduction of the carbon content at 500ºC sintering condition (1.47 wt%) evidently showed that the additional UV-O_3 treatment is very critical to eliminating the carbon residues after sintering at relatively low temperatures. The thermogram in Fig. 2d exhibited a continuous weight loss up to 62 and 51.75%, respectively, for $\mathbf{P_{BL}}$ and $\mathbf{P_O}$ at 138ºC, while no further significant weight loss was observed until 500ºC (63.50 and 53.15%, respectively, for $\mathbf{P_{BL}}$ and $\mathbf{P_O}$), consistent with the previous weight loss data. The little high residual percentage of $\mathbf{P_O}$ compared to $\mathbf{P_{BL}}$ can be ascribed to the incomplete removal of 1-octanol from $\mathbf{P_O}$ induced by its high T_b (194.5ºC). These results demonstrated that both $\mathbf{P_{BL}}$ and $\mathbf{P_O}$ pastes are suitable for the preparation of binder-free *f*-DSSCs photoanodes under low-temperature sintering conditions with subsequent UV-O_3 treatment. Additionally, the crystallographic pattern of the TiO_2 NPs in the $\mathbf{P_{BL}}$ and $\mathbf{P_O}$-based TiO_2

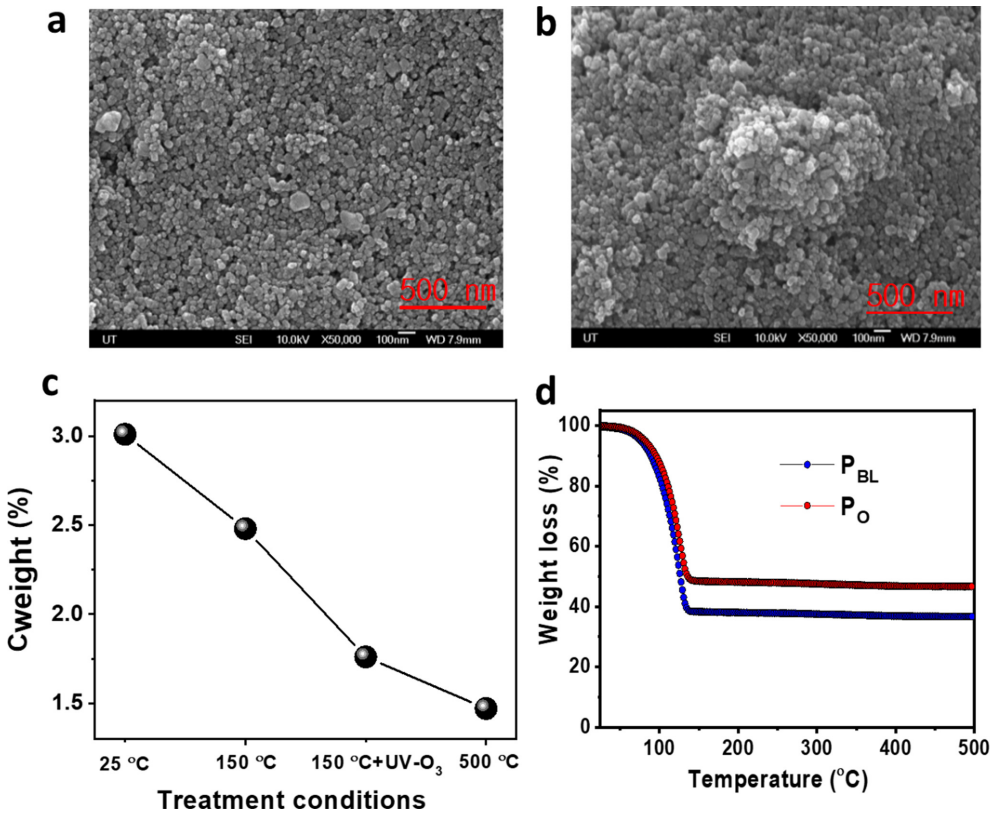

Fig. 2. Top-view FE-SEM images of (a) $\mathbf{P_{BL}}$ and (b) $\mathbf{P_O}$ pastes-based TiO_2 films after sintering at 150ºC and subsequent UV-O_3 treatment. (c) Weight (%) of carbon in the TiO_2 film of $\mathbf{P_{BL}}$ with different treatment conditions. (d) TGA curve of RT dried TiO_2 pastes with a heating range of 3ºC/min.

films exhibited that anatase is the major crystal phase (JCPDS card no. 21-1272) (Fig. S6) [33]. This is advantageous for improved dye-loading and the development of high-performance DSSCs [34].

3.4. Photovoltaic characterizations

Fig. 3a presents the photo-current density-voltage (J-V) plots of the *g*-DSSCs based on the TiO_2 photoanodes of $\mathbf{P_{BL}}$ **and** $\mathbf{P_O}$, sintered at 150ºC. The resulting PV parameters are summarized in Table 1. It was observed that the $\mathbf{P_O}$ cell showed the lowest PV performance with the short-circuit current density (J_{sc}), open-circuit potential (V_{oc}), and PCE of 8.45 mA/cm^2, 0.73 V, and 4.2%, respectively. Meanwhile, the $\mathbf{P_{BL}}$ cell exhibited the PCE enhancement of 30% compared to the $\mathbf{P_O}$ cell with the J_{sc}, V_{oc}, and PCE of 12.07 mA/cm^2, 0.73 V, and 6.0%, respectively. The increase in the PCE of $\mathbf{P_{BL}}$ cell compared to the $\mathbf{P_O}$ device is mostly due to the increase in J_{sc}. This can be attributed to the improved dye loading in $\mathbf{P_{BL}}$ (2.51×10^{-8} mol/cm^2) compared to the $\mathbf{P_O}$ (ca. 1.8×10^{-8} mol/cm^2) (Fig. S7a). The high visible transparency of the TiO_2 film of $\mathbf{P_{BL}}$ compared to the $\mathbf{P_O}$ film (Fig. S7b) is another possible reason for increased J_{sc}. Meanwhile, the 500ºC sintered $\mathbf{P_{BL}}$-based *g*-DSSC exhibited a PCE of 6.3%, which is comparable to the PCE of $\mathbf{P_C}$ cell (7.10%) (Fig. 3b and Table 1). The improved PV performance of the $\mathbf{P_C}$-based *g*-DSSCs is due to the enhanced TiO_2 interparticle connection compared to $\mathbf{P_{BL}}$, which corroborates a 24.32% higher J_{sc}. This result suggests that $\mathbf{P_{BL}}$ is promising to develop conventional high-temperature sintered *g*-DSSCs.

Finally, *f*-DSSCs were fabricated by utilizing $\mathbf{P_{BL}}$ and $\mathbf{P_O}$ on ITO/PEN substrate, and the resulting J-V plots and PV parameters are summarized in Fig. 3c and Table 1, respectively. Similar to the *g*-DSSCs, the fully flexible cell with $\mathbf{P_{BL}}$ exhibited a PCE of 3.5% with the J_{sc}, V_{oc}, and *FF* of 9.42 mA/cm^2, 0.70 V, and

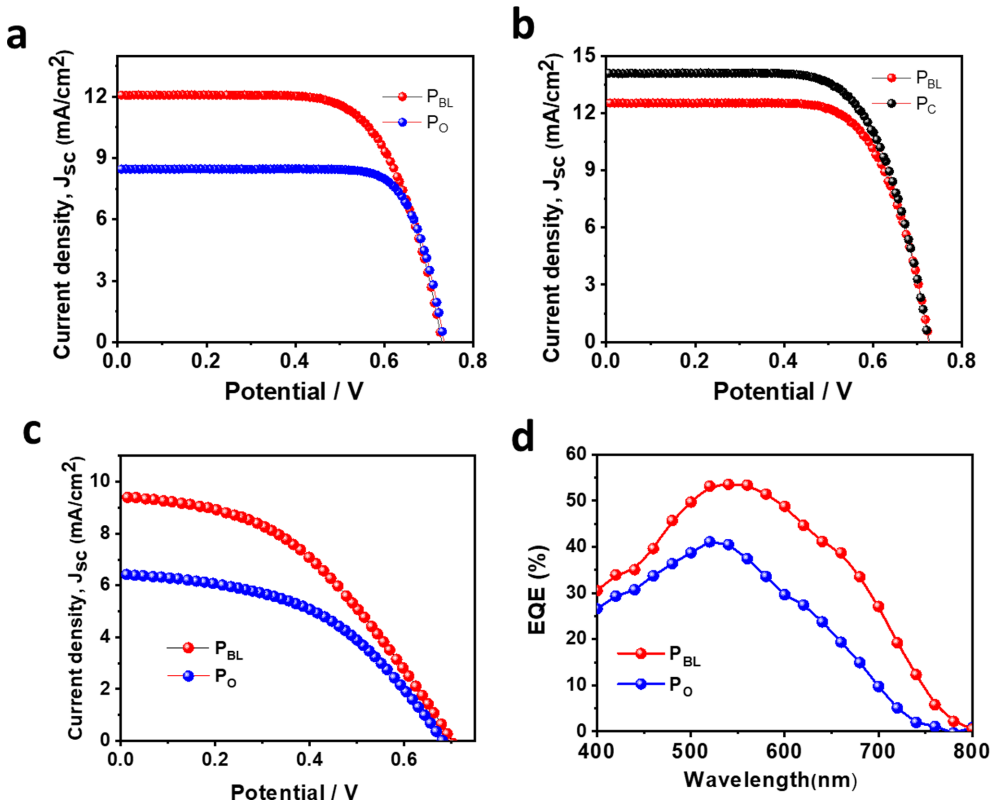

Fig. 3. Photo-current density (J) - voltage (V) characteristics of different TiO_2 paste based *g*-DSSCs sintered at (a) 150ºC and (b) 500ºC, and (b) *f*-DSSCs sintered at 150ºC. (d) The IPCE spectra of the corresponding *f*-DSSCs.

Table 1. Photovoltaic parameters of different TiO_2 pastes based DSSCs.

Substrate	Pastes	Sintering temp. (ºC)	V_{oc} (V)	J_{sc} (mA/cm^2)	*FF* (%)	*PCE* (%)
Glass/FTO	P_{BL}	150	0.73	12.07	68.0	6.0
	P_O	150	0.73	8.45	68.1	4.2
	P_{BL}	500	0.73	12.52	69.8	6.3
	P_C	500	0.70	15.95	68.8	7.1
ITO/PEN	P_{BL}	150	0.70	9.42	52.3	3.5
	P_O	150	0.68	6.42	46.8	2.0

52.3%, respectively, while the PCE was 2.0% for **P_O** with the J_{sc}, V_{oc}, and *FF* of 6.42 mA/cm^2, 0.68 V, and 46.8%, respectively. By inspection, the 75% PCE enhancement for **P_{BL}**-based *f*-DSSC compared to the **P_O** device is mainly due to the significant increase of J_{sc} (46.72% enhancement). This can be attributed to the improved TiO_2 interparticle connection and dye loading of the **P_{BL}**-based TiO_2 film compared to the TiO_2 film based on **P_O**. Nevertheless, The PCE of the **P_{BL}**-based *f*-DSSC is 71.40% lower than the *g*-DSSC prepared under similar conditions. This can be ascribed to the high ohmic resistance of the ITO/PEN substrate as well as the internal resistance of the devices, which corroborated a significantly low FF. The PCE of the **P_{BL}** DSSC is higher or comparable to the previously reported *g*-DSSCs and *f*-DSSCs prepared under low-temperature sintering conditions (Table S1), suggesting that **P_{BL}** can be effectively uti-

lized for developing high-performance DSSCs with additional electrode engineering. Fig. 3d shows the IPCE spectra of the corresponding *f*-DSSCs based on $\mathbf{P_{BL}}$ and $\mathbf{P_O}$. It can be observed that the external quantum efficiency (EQE) of the $\mathbf{P_{BL}}$ cell exhibited an upward shift over the wide wavelength range (400–800 nm) with the maximum EQE value of 54% at 540 nm, while this value for the $\mathbf{P_O}$ device was 41% at 540 nm. This result is consistent with the J_{sc} values of the corresponding *f*-DSSCs devices.

3.5. Electrochemical characterizations

EIS spectra of the $\mathbf{P_{BL}}$ and $\mathbf{P_O}$-based *f*-DSSCs were measured to investigate the electron transport mechanism and the interfacial properties. Fig. 4 shows the EIS spectra of the devices in the form of Nyquist plots, which exhibited three semicircles. The semicircle at the high-, mid-, and low-frequency regions corresponds to the charge transfer resistance at the CE/electrolyte interface (R_{ct1}), charge transfer resistance at the TiO_2/dye/electrolyte interface (R_{ct2}), and the diffusion resistance ($Z_{diffusion}$) within the electrolyte, respectively [35]. The intercept with the real axis at the high-frequency region corresponds to the contact resistance (R_s) between the TiO_2/substrate or the ohmic resistance of the cells [35,36]. Generally, the R_s values do not alter much in a DSSC with similar substrates and paste. However, a little lower R_s for the $\mathbf{P_{BL}}$ cell (13.2 W) than the $\mathbf{P_O}$-based *f*-DSSC (14.4 W) suggests the lower contact resistance between the $\mathbf{P_{BL}}$ TiO_2 film and ITO/PEN substrates. This can be attributed to the strong adhesion of the $\mathbf{P_{BL}}$ TiO_2 film with the substrate [36], consistent with the scotch tape and mechanical adhesion tests. The R_{ct2} values for $\mathbf{P_{BL}}$ and $\mathbf{P_O}$ devices are 21.36 and 27.49 W, respectively. The lower R_{ct2} designates the faster interfacial charge transfer process and lower recombination in the $\mathbf{P_{BL}}$ device compared to the $\mathbf{P_O}$ device [35], which is consistent with the PV parameters of their corresponding *f*-DSSC.

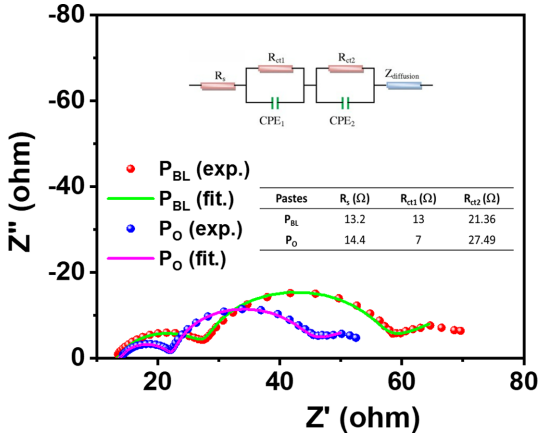

Fig. 4. Nyquist plots of *f*-DSSCs measured under open circuit and dark conditions. The upper inset shows the equivalent circuit model to fit the spectra, and the table in the lower inset displays the fitted results of EIS parameters.

4. Conclusions

This study described the utilization of 1-octanol with high viscosity and high T_b together with CCl_4 with low viscosity and low T_b to prepare a binder-free TiO_2 paste for low-temperature sintered *f*-DSSCs. The 1:1 (v/v) complex of CCl_4 and 1-octanol could interact with the TiO_2 NPs via hydrogen bonding, which reduced the TiO_2 interparticle distance and formed a vicious TiO_2 paste. This binary-liquid-based TiO_2 paste, $\mathbf{P_{BL}}$, exhibited strong adhesion to the FTO/glass and ITO/PEN substrates with high mechanical stability. The $\mathbf{P_{BL}}$-based *f*-DSSC and *g*-DSSC, sintered at 150 and 500ºC, respectively, exhibited PCEs of 3.5 and 6.3%, respectively. The PCE for *f*-DSSC and *g*-DSSC based on pure 1-octanol paste and sintered at 150ºC, were 2.0 and 4.0%, respectively, while this value for commercial 500ºC sintered $\mathbf{P_C}$-based *g*-DSSC was 7.1%. The significantly improved PCE of $\mathbf{P_{BL}}$-based *f*-DSSC and *g*-DSSC compared to the pure 1-octanol paste-based cells can be attributed to the strong adhesion and high mechanical stability of the corresponding TiO_2 film with improved porosity and dye loading. This result demonstrated the applicability of the $\mathbf{P_{BL}}$ paste for the development of both low- and high-temperature sintered DSSCs. We strongly believe that the present methodology is promising for developing high-efficiency *f*-DSSCs by choosing other highly viscous alcohols and low boiling temperature liquids.

Acknowledgements

This research was supported by the Technology Development Program to Solve Climate Changes of the National Research Foundation, funded by the Ministry of Science, ICT & Future Planning (NRF-2016M1A2A2940912).

Supporting information

Supporting Information is available at https://doi.org/10.33961/jecst.2022.00262

References

[1] B. O'Regan and M. Grätzel, *Nature*, **1991**, *353*, 737-740.
[2] K. Sharma, V. Sharma, and S. S. Sharma, *Nanoscale Res. Lett.*, **2018**, *13*, 381.
[3] D. Devadiga, M. Selvakumar, P. Shetty, and M. S. Santosh, *J. Power Sources*, **2021**, *493*, 229698.
[4] K. Kakiage, Y. Aoyama, T. Yano, K. Oya, J. Fujisawa, and M. Hanaya, *Chem. Commun.*, **2015**, *51*, 15894-15897.
[5] J.-M. Ji, H. Zhou, Y. K. Eom, C. H. Kim, and H. K. Kim, *Adv. Energy Mater.*, **2020**, *10(15)*, 2000124.
[6] G. Li, L. Sheng, T. Li, J. Hu, P. Li, and K. Wang, *Sol. Energy*, **2019**, *177*, 80-98.
[7] H. C. Weerasinghe, F. Huang, and Y.-B. Cheng, *Nano Energy*, **2013**, *2(2)*, 174-189.
[8] K. Kim, G. W. Lee, K. Yoo, D. Y. Kim, J. K. Kim, and N. G. Park, *J. Photochem. Photobiol. A: Chem.*, **2009**, *204(2-3)*, 144-147.
[9] S. Sarker, N. C. D. Nath, M. M. Rahman, S.-S. Lim, A. J. S. Ahammad, W.-Y. Choi, and J.-J. Lee, *J. Nanosci. Nanotechnol.*, **2012**, *12(7)*, 5361-5366.
[10] M. M. Rahman, H.-Y. Kim, Y.-D. Jeon, I.-S. Jung, K.-M. Noh, and J.-J. Lee, *Bull. Korean Chem. Soc.*, **2013**, *34(9)*, 2765-2768.
[11] M. M. Rahman, H.-S. Son, S.-S. Lim, K.-H. Chung, and J.-J. Lee, *J. Electrochem. Sci. Technol.*, **2011**, *2(2)*, 110-115.
[12] H.-P. Jen, M.-H. Lin, L.-L. Li, H.-P. Wu, W.-K. Huang, P.-J. Cheng, and E. W.-G. Diau, *ACS Appl. Mater. Interfaces*, **2013**, *5(20)*, 10098-10104.
[13] T. Yamaguchi, N. Tobe, D. Matsumoto, T. Nagai, and H. Arakawa, *Sol. Energy Mater. Sol. Cells*, **2010**, *94(5)*, 812-816.
[14] G. Boschloo, H. Lindstrom, E. Magnusson, A. Holmberg, and A. Hagfeldt, *J. Photochem. Photobiol. A*, **2002**, *148(1-3)*, 11-15.
[15] J. H. Yum, S. S. Kim, D. Y. Kim, and Y. E. Sung, *J. Photochem. Photobiol. A*, **2005**, *173(1)*, 1-6.
[16] L. Grinis, S. Kotlyar, S. Ruhle, J. Grinblat, and A. Zaban, *Adv. Funct. Mater.*, **2010**, *20(2)*, 282-288.
[17] H. W. Chen, C. P. Liang, H. S. Huang, J. G. Chen, R. Vittal, C. Y. Lin, C. W. W. Kevin, and K. C. Ho, *Chem. Commun.*, **2011**, *47*, 8346-8348.
[18] S. Uchida, M. Tomiha, H. Takizawa, and M. Kawaraya, *J. Photochem. Photobiol. A*, **2004**, *164(1-3)*, 93-96.
[19] S. I. Cha, B. K. Koo, K. H. Hwang, S. H. Seo, and D. Y. Lee, *J. Mater. Chem.*, **2011**, *21*, 6300-6304.
[20] X. Li, H. Lin, J. Li, N. Wang, C. Lin, and L. Zhang, *J. Photochem. Photobiol. A*, **2008**, *195(2-3)*, 247-253.
[21] N.-G. Park, K. M. Kim, M. G. Kang, K. S. Ryu, S. H. Chang, and Y.-J. Shin, *Adv. Mater.*, **2005**, *17(19)*, 2349-2353.
[22] M. Dürr, A. Schmid, M. Obermaier, S. Rosselli, A. Yasuda, and G. Nelles, *Nat. Mater.*, **2005**, *4*, 607-611.
[23] Y. Li, W. Lee, D.-K. Lee, K. Kim, N.-G. Park, and M. J. Ko, *Appl. Phys. Lett.*, **2011**, *98*, 103301.
[24] J. H. Yune, I. Karatchevtseva, G. Triani, K. Wagner, and D. Officer, *J. Mater. Res.*, **2013**, *28(3)*, 488-496.
[25] H. C. Weerasinghe, P. M. Sirimanne, G. V. Franks, G. P. Simon, and Y. B. Cheng, *J. Photochem. Photobiol. A: Chem.*, **2010**, *213(1)*, 30-36.
[26] P. J. Holliman, A. Connell, M. Davis, M. Carnie, D. Bryant, and E. W. Jones, *Mater. Lett.*, **2019**, *236*, 289-291.
[27] F.-M. Raoult, *C. R. Hebd. Séances Acad. Sci.*, **1887**, *104*, 1430-1433.
[28] M. M. Rahman, M. J. Ko, and J.-J. Lee, *Nanoscale*, **2015**, *7*, 3526-3531.
[29] M. M. Rahman, S. Y. Im, and J.-J. Lee, *Nanoscale*, **2016**, *8*, 5884-5891.
[30] A. N. Fletcher, *J. Phys. Chem.*, **1969**, *73(7)*, 2217-2225.
[31] L. N. Lewis, J. L. Spivack, S. Gasaway, E. D. Williams, J. Y. Gui, V. Manivannan, and O. P. Siclovan, *Sol. Energy Mater. Sol. Cells*, **2006**, *90(7-8)*, 1041-1051.
[32] Y.-S. Lin, M.-T. Chen, Y.-F. Lin, S.-J. Yang, and J.-L. Lin, *Appl. Surf. Sci.*, **2006**, *252(16)*, 5892-5899.
[33] K.-H. Chung, M. M. Rahman, H.-S. Son, and J.-J. Lee, *Int. J. Photoenergy*, **2012**, *2012*, 215802.
[34] J.-J. Lee, M. M. Rahman, S. Sarker, N. C. Deb Nath, A.J. S. Ahammad, and J. K. Lee, B. Attaf(Ed.), in *Composite materials for medicine and nanotechnology*, Intech, Croatia, **2011**, 181.
[35] M. M. Rahman, N. C. D. Nath, and J.-J. Lee, *Isrl. J. Chem.*, **2015**, *55(9)*, 990-1001.
[36] M. M. Rahman, *Materials*, **2021**, *14(21)*, 6563.